PIECEWISE SMOOTH SEGMENTATION WITH SPARSE PRIOR*

*Yutong Li and Yuping Duan**

Center for Applied Mathematics, Tianjin University

ABSTRACT

Exploiting sparsity in the image gradient magnitude has proved effective in preserving sharp edges and reducing noises for many image processing tasks. Based on observation, we build up a novel piecewise smooth segmentation model by utilizing a generalized total variation (TV) prior with p-th power for $0 < p < 1$ and a ℓ^1 data fidelity. We present an efficient algorithm based on the alternating direction method of multipliers (ADMM), where all subproblems can be solved by either one-step Gauss-Seidel iteration or the closed-form solution. Numerical experiments show that the proposed model can achieve more accurate segmentation results than the classical TV based segmentation model.

***Index Terms*—** Image segmentation, intensity inhomogeneity, total variation regularization, ℓ^p minimization, ADMM

1. INTRODUCTION

Image segmentation is an important task in image processing, which decomposes the image domain into local regions according to the features such as intensities, edges, colors and so on. Intensity inhomogeneity is a commonly seen artifact in natural image and medical image due to the spatial variation in illuminations and imperfection of imaging devices. The existence of intensity inhomogeneity makes the segmentation algorithms that relying on the assumption of uniform intensity impossible to identify the regions correctly.

Mumford and Shah [1] proposed the most fundamental region-based model for image segmentation, which can deal with intensity inhomogeneous images. Let $\Omega \in \mathbb{R}^2$ be open and bounded, and Γ be a closed subset in Ω. Given an observed image $I : \Omega \to \mathbb{R}$, the MS model finds its piecewise smooth approximation u by solving the following minimization problem

$$\min_{u,\Gamma} \lambda \int_{\Omega} (I-u)^2 dx + \beta \int_{\Omega\setminus\Gamma} |\nabla u|^2 dx + |\Gamma|, \qquad (1)$$

where λ and β are positive parameters and $|\Gamma|$ denotes the length of Γ. Because the Mumford-Shah functional is nonconvex and the integral regions of last two terms are discontinuous, finding the minimizers is not straightforward and may trap into local minima.

Many variants have been proposed for efficient implementation of the MS model. Chan and Vese [2] sought for a binary approximation of the given image through a level set formulation [3], which has also been extended for multiphase segmentation in [4]. Lie *et al.* [5] proposed the piecewise constant level set method to identify curves separating regions into different phases. Chan *et al.* [6] reformulated the CV model into an equivalent convex minimization, which makes convex optimization techniques be applicable for image segmentation problems. Similar idea has been utilized for multi-phase segmentation in [7, 8]. Because such piecewise constant models approximate the image domain by a set of homogeneous regions, they fail in segmenting images with intensity inhomogeneity.

Piecewise smooth (PS) segmentation models perform better for intensity inhomogeneous images. Le and Vese [9] proposed a piecewise smooth segmentation model by expressing the true intensity as a summation of a piecewise constant component and a smooth component, i.e.,

$$g = \sum_{i=1}^{N} c_i \chi_i + b, \qquad (2)$$

where $b : \Omega \to \mathbb{R}$ is a spatially smooth function modeling the intensity inhomogeneity, χ_i is the characteristic function of set Ω_i and $\{c_i\}_{i=1}^N$ are constant values representing the mean value of intensity inside $\{\Omega_i\}_{i=1}^N$. Based on (2), Jung [10] used the ℓ^1 data fidelity to reformulate the energy functional for better segmentation of images with low contrast or outliers. Indeed, the relationship between the piecewise constant function and the smooth function may be modelled in a multiplicative intrinsic [11, 12].

The aforementioned methods are all based on the total variation (TV) semi-norm, which is defined as the ℓ^1 norm of the image gradient magnitude. It is well-known the ℓ^1 norm promotes sparsity in its arguments by preserving the edges of the images as well as eliminating the noises. Indeed, a better choice to enhance the sparsity is to employ the ℓ^p quasi-norm for $0 < p < 1$, which has already been used for image restoration [13], image reconstruction [14] etc. As only the boundaries between adjacent regions need to be measured for segmentation tasks, we propose a novel PS segmentation model by minimizing the ℓ^p norm of image gradient magnitudes, the so-called TV$_p$ norm. We adopt the ℓ^1 data fidelity as it was proven efficient in dealing with images with low contrast

THE WORK IS SUPPORTED BY THE 1000 TALENTS PROGRAM FOR YOUNG SCIENTISTS OF CHINA, AND NSFC 11701418.

* Corresponding author: yuping.duan@tju.edu.cn.

[10]. An effective algorithm is developed based on the ADMM strategy, where all subproblems can be solved by either one-step Gauss-Seidel iteration or closed-form solution. Numerical experiments on two-phase and multiphase segmentation are presented, which demonstrate the superiority of the TV_p regularization over the classical TV based model.

2. PROBLEM FORMULATION

Without loss of generality, we assume u as a grayscale image of the size $d \times d$ and have the following definition of TV_p regularization in the discrete setting

$$TV_p(u) := \sum_{i=1}^{d\times d} \|(\nabla u)_i\|_2^p, \text{ with } 0 < p < 1. \tag{3}$$

Based on the image model (2), we propose the following TV_p regularized minimization problem for piecewise smooth image segmentation

$$\min_{\boldsymbol{u},b,\boldsymbol{c}} \lambda \sum_{i=1}^{N} \langle |I - c_i - b|, R_i\rangle + \sum_{l=1}^{m} \|\nabla u_l\|_2^p + \mu\|\nabla b\|_2^2, \tag{4}$$

where $u_l \in [0,1]$, $\forall l = 1,\ldots,m$ and R_i represents the subregion Ω_i satisfying $\sum_{i=1}^N R_i = 1$ with $N = 2^m$. More specifically, we have $R_1 = u$, $R_2 = (1-u)$ for $N = 2$, and $R_1 = u_1u_2$, $R_2 = u_1(1-u_2)$, $R_3 = (1-u_1)u_2$, $R_4 = (1-u_1)(1-u_2)$ for $N = 4$, and so forth.

The natural way to compute the solution of (4) is to use an alternative scheme to minimize each variable iteratively and alternatively.

2.1. Sub-minimization problem w.r.t. $(\boldsymbol{c}, b)$

We use the variable splitting technique to separate the ℓ^1 norm and ℓ^2 norm in the minimization, where an auxiliary variable $\boldsymbol{p} = (p_1,\ldots,p_N)$ is introduced as follows

$$\min_{\boldsymbol{c},b,\boldsymbol{p}} \lambda \sum_{i=1}^{N} \langle |p_i|, R_i\rangle + \mu\|\nabla b\|_2^2, \text{ s.t. } \boldsymbol{p} = I - \boldsymbol{c} - b, \tag{5}$$

which can be reformulated into a saddle-point problem based on the augmented Lagrangian method

$$\mathcal{L}(\boldsymbol{c}, b, \boldsymbol{q}; \boldsymbol{\eta}) = \lambda \sum_{i=1}^{N} \langle |p_i|, R_i\rangle + \mu\|\nabla b\|_2^2$$
$$- \sum_{i=1}^{N} \Big(\langle \eta_i, p_i - (I - c_i - b)\rangle - \tfrac{\tau}{2}\|p_i - (I - c_i - b)\|_2^2 \Big),$$

where $\boldsymbol{\eta}$ is the Lagrange multiplier and τ is a positive parameter. We employ the splitting technique by calculating $\boldsymbol{c}$, b and $\boldsymbol{p}$ separately as follows

$$\min_{\boldsymbol{c}} \ \frac{\tau}{2}\Big\|\boldsymbol{c} - (I - b - \boldsymbol{p} + \frac{\boldsymbol{\eta}}{\tau})\Big\|_2^2, \tag{6}$$

for given b and $\boldsymbol{p}$, and

$$\min_{b} \ \mu\|\nabla b\|_2^2 + \frac{\tau}{2}\sum_{i=1}^{N} \|p_i - (I - c_i - b) - \frac{\eta_i}{\tau}\|_2^2, \tag{7}$$

for given $\boldsymbol{p}$ and $\boldsymbol{c}$, and

$$\min_{\boldsymbol{p}} \sum_{i=1}^{N} \Big(\lambda\langle |p_i|, R_i\rangle + \frac{\tau}{2}\|p_i - (I - c_i - b) - \frac{\eta_i}{\tau}\|_2^2 \Big), \tag{8}$$

for given b and $\boldsymbol{c}$.

The optimality condition of (6) gives us the following closed-form solution

$$c_i = \frac{\int_\Omega I - b - p_i + \frac{\eta_i}{\tau} dx}{\int_\Omega dx}, \quad \text{for } i = 1,\ldots,N. \tag{9}$$

For (7), the Euler-Lagrange equation gives a linear equation

$$(\tau N - 2\mu\Delta) b = \tau \sum_{i=1}^{N} (I - c_i - p_i + \frac{\eta_i}{\tau}), \tag{10}$$

which can be solved by the discrete Fast Fourier transform (FFT) under the periodic boundary condition, i.e.,

$$b = \mathcal{F}^{-1}\bigg(\frac{\mathcal{F}\big(\tau\sum_{i=1}^N (I - c_i - p_i + \frac{\eta_i}{\tau})\big)}{(\tau N - 2\mu\mathcal{F}(\Delta))} \bigg). \tag{11}$$

For (8), after the elementary calculations of the optimality condition, we can obtain a closed-form solution as

$$p_i = \operatorname{shrink}\big(I - c_i - b + \frac{\eta_i}{\tau}, \frac{\lambda R_i}{\tau}\big), \tag{12}$$

where $\operatorname{shrink}(s_\alpha, t_\alpha) = \frac{s_\alpha}{|s_\alpha|}\max(|s_\alpha| - t_\alpha, 0)$.

2.2. Sub-minimization problem w.r.t. $\boldsymbol{u}$

The subproblem of $\boldsymbol{u}$ is a constrained minimization problem as follows

$$\min_{\boldsymbol{u}} \ \lambda \sum_{i=1}^{N} \langle f_i, R_i\rangle + \sum_{l=1}^{m} \|\nabla u_l\|_2^p, \quad u_l \in [0,1], \tag{13}$$

where $f_i = |f - c_i - b|$. The energy functional in (13) has multi-variables $u_1,\ldots,u_m$, which can be solved individually. Thus, we compute each u_l by minimizing the functional with respect to u_l while the others are fixed

$$\min_{u_l\in[0,1]} \ \lambda\langle r_l, u_l\rangle + \|\nabla u_l\|_2^p, \quad \text{for } l = 1,\ldots,m, \tag{14}$$

where $r_1 = f_1 - f_2$ for $N = 2$ and $r_1 = (f_1 - f_3)u_2 + (f_2 - f_4)(1-u_2)$, $r_2 = (f_1 - f_2)u_1 + (f_3 - f_4)(1-u_1)$ for $N = 4$, and so forth.

For simplicity, we denote $r = r_l$ and $u = u_l$. By introducing a new variable $\boldsymbol{q}$, the subproblem (14) becomes

$$\min_{u\in[0,1]} \quad \lambda\langle r, u\rangle + \|\boldsymbol{q}\|_2^p, \qquad \text{s.t. } \boldsymbol{q} = \nabla u. \tag{15}$$

Based on the augmented Lagrangian method, we can reformulate the constrained optimization problem (15) into an equivalent saddle-point problem as follows

$$\mathcal{L}_u(u, \boldsymbol{q}; \boldsymbol{\xi}) = \lambda\langle r, u\rangle + \|\boldsymbol{q}\|_2^p - \langle \boldsymbol{\xi}, \boldsymbol{q} - \nabla u\rangle + \frac{\gamma}{2}\|\boldsymbol{q} - \nabla u\|_2^2,$$

where $\boldsymbol{\xi}$ is the Lagrange multiplier and γ is a positive parameter. Similarly, two subproblems are solved instead of the saddle-point problem

$$\min_u \quad \lambda\langle r, u\rangle + \frac{\gamma}{2}\|\boldsymbol{q} - \nabla u - \frac{\boldsymbol{\xi}}{\gamma}\|_2^2, \tag{16}$$

for a given $\boldsymbol{q}$ and $\boldsymbol{\xi}$, and

$$\min_{\boldsymbol{q}} \quad \|\boldsymbol{q}\|_2^p + \frac{\gamma}{2}\|\boldsymbol{q} - \nabla u - \frac{\boldsymbol{\xi}}{\gamma}\|_2^2, \tag{17}$$

for a given u.

For (16), the optimality condition gives the following linear equation

$$\gamma\Delta u = \lambda r + \gamma \mathrm{div}(\boldsymbol{q} - \frac{\boldsymbol{\xi}}{\gamma}), \tag{18}$$

which can be efficiently solved by one-step Gauss-Seidel iteration. Denote $T_{i,j} = q_{i,j}^{x,k} + q_{i-1,j}^{x,k} + q_{i,j}^{y,k} + q_{i,j-1}^{y,k} - \frac{1}{\gamma}(\xi_{i,j}^{x,k} + \xi_{i-1,j}^{x,k} + \xi_{i,j}^{y,k} + \xi_{i,j-1}^{y,k})$. The solution of u is achieved by

$$u_{i,j}^{k+1} = \frac{1}{4}\big((u_{i+1,j}^{k+1} + u_{i-1,j}^{k+1} + u_{i,j+1}^{k+1} + u_{i,j-1}^{k+1}) - T_{i,j} - \frac{\lambda}{\gamma} r_{i,j}\big) \tag{19}$$

with a projection step on u^{k+1} to restrict its value to $[0, 1]$.

In the end, we calculate (17) explicitly according to the following proposition.

Proposition 2.1 *([13]) Let $0 < p < 1$. The solution to minimization problem* (17) *is given by*

$$\boldsymbol{q} = \eta^*(\nabla u + \frac{\boldsymbol{\xi}}{\gamma}), \quad \textit{where} \quad \eta^* \in [0, 1], \tag{20}$$

with

$$\begin{cases} \eta^* = 0, & \textit{if } \omega \leq \overline{\omega}, \\ \eta^* = \dfrac{p(p-2) + \omega}{p(p-1) + \omega}, & \textit{if } \omega > \overline{\omega}, \end{cases}$$

where we set

$$\omega := \gamma\big\|\nabla u + \frac{\boldsymbol{\xi}}{\gamma}\big\|_2^{2-p}, \quad \overline{\omega} := \frac{(2-p)^{2-p}}{(2-2p)^{1-p}}.$$

We conclude this section with the alternating minimization algorithm for solving (4); see Algorithm I.

Algorithm I: Alternating minimization algorithm for (4)

Initialize: choose λ, μ, τ, $\gamma > 0$, and let $b = p_i^0 = \eta_i^0 = 0$ for $i = 1, \dots, N$; $\mathbf{q}_l^0 = \boldsymbol{\xi}_l^0 = \mathbf{0}$, for $l = 1, ..., m$; $u_l^0 = 1$ in some reign, $u_l^0 = 0$ otherwise.

Iterate for $k = 0, 1, 2, \dots$:

- With $\boldsymbol{p}^k$, b^k and $\boldsymbol{\eta}^k$, solve $\boldsymbol{c}^{k+1}$ from (9);
- With $\boldsymbol{p}^k$, $\boldsymbol{c}^{k+1}$ and $\boldsymbol{\eta}^k$, solve b^{k+1} from (11);
- With $\boldsymbol{u}^k$, $\boldsymbol{c}^{k+1}$, b^{k+1} and $\boldsymbol{\eta}^k$, solve $\boldsymbol{p}^{k+1}$ from (12);
- With $\boldsymbol{q}^k$ and $\boldsymbol{\xi}^k$, solve $\boldsymbol{u}^{k+1}$ from (19);
- With $\boldsymbol{u}^{k+1}$ and $\boldsymbol{\xi}^k$, solve $\boldsymbol{q}^{k+1}$ from (20);
- Update Lagrange multiplier $\boldsymbol{\eta}$ and $\boldsymbol{\xi}$ from

$$\begin{aligned} \boldsymbol{\eta}^{k+1} &= \boldsymbol{\eta}^k - \tau(\boldsymbol{p}^{k+1} - (I - \boldsymbol{c}^{k+1} - b^{k+1})); \\ \boldsymbol{\xi}^{k+1} &= \boldsymbol{\xi}^k - \gamma(\mathbf{q}^{k+1} - \nabla\boldsymbol{u}^{k+1}). \end{aligned}$$

3. NUMERICAL EXPERIMENTS

This section presents the numerical results of the proposed PS model of TV_p regularization and compare the results with the PS model of TV regularization [10][1], which are denoted as TVp model and TV model, respectively. We give the following two remarks before illustrating our results:

1. We use the Jaccard Similarity (JS) to quantitatively evaluate the segmentation accuracy, which is defined as $JS(S_1, S_2) = \frac{|S_1 \cap S_2|}{|S_1 \cup S_2|}$, where S_1 is the region segmented by the algorithm and S_2 is the corresponding region in the ground truth.
2. Both algorithms are terminated when either the maximum iteration number exceeds $K = 1000$, or the relative error is reached as $\frac{\|\boldsymbol{c}^{k+1} - \boldsymbol{c}^k\|_2}{\|\boldsymbol{c}^{k+1}\|_2} < \epsilon$ with $\epsilon = 10^{-6}$.

3.1. Two-phase segmentation

Firstly, we test our model on two grayscale images. As shown in Fig. 1 and Fig. 2, different intensity inhomogeneities from small to large are introduced into the test images. We set p as $p = 1/3$, $p = 1/2$, $p = 2/3$ in the TVp model. We can observe that both TVp model and TV model can well segment the images when the intensity inhomogeneity is small. As the degree of nonuniformity increases, the superiority of the TVp model becomes more pronounced, which can preserve corners and curves of the images. Meanwhile, we tabulate the JS values of both TVp model and TV model in Table 1, the values of which correspond to the visual results. Better JS values can be achieved by TVp model and JS values are slightly improved as the sparsity increases. Thus, we can select p as $p = 1/3$ in the applications.

Table 1. JS of synthetic images.

Methods	Fig. 1			Fig. 2		
	1^{st} row	2^{nd} row	3^{rd} row	1^{st} row	2^{nd} row	3^{rd} row
$p = 1/3$	100	99.95	99.71	97.79	97.76	97.40
$p = 1/2$	100	99.85	99.71	97.79	97.74	97.36
$p = 2/3$	100	99.85	99.71	97.74	97.72	97.29
TV model	100	99.71	97.83	97.73	97.70	95.10

Secondly, we present an example of our TVp model on noisy image. Fig. 3 illustrates that the proposed model can achieve better or comparable segmentation results as TV model when the original images are corrupted by both noises and intensity inhomogeneity.

3.2. Multi-phase segmentation

In this subsection, we test our model on two brain images, both of which have slowly varying intensities inside the brain. As there mainly exists three different tissues, i.e., white matter (WM), gray matter (GM) and cerebrospinal fluid (CSF), we implement a four phase segmentation model. In Fig. 4 and Fig. 5, we present the original image, the initialization of

[1] The authors would like to thank Prof. Miyoun Jung from Hankuk University of Foreign Studies for providing us with MATLAB code of L1 model [10].

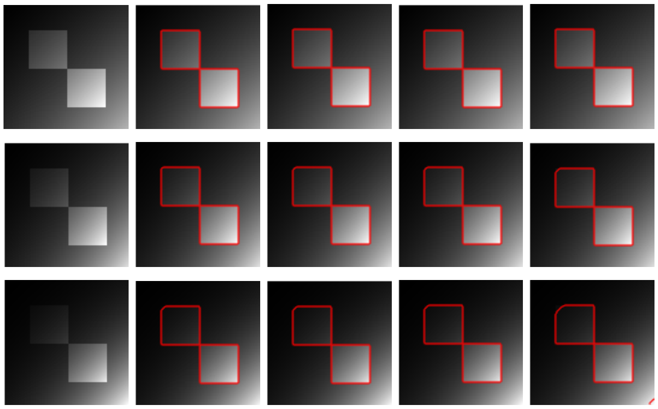

Fig. 1. From left to right: the original image, the segmentation results of TVp model with p=1/3, 1/2, 2/3 and TV model.

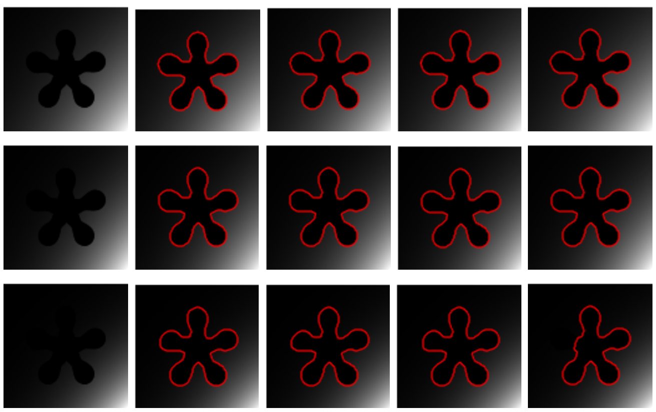

Fig. 2. From left to right: the original image, the segmentation results of TVp model with p=1/3, 1/2, 2/3 and TV model.

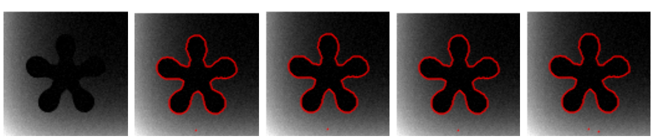

Fig. 3. From left to right: the original image, the segmentation results of TVp model with p=1/3, 1/2, 2/3 and TV model.

level set functions, the piecewise smooth image g, the final membership functions u_1, u_2, and the segmentation results of WM, GM, CSF generated by u_1 and u_2.

As shown by 4, the TV model struggles to segment the left part of the brain, while our model can achieve a better segmentation of WM. Simultaneously, the JS values in Table 2 demonstrate that the segmentation result of our TVp model is more accurate than TV model. In Fig.5, obvious inhomogeneous intensities can be observed in the top part of the brain. The comparison shows that TV model classified the top part as GM while our TVp model correctly identified the boundary between WM and GM. Compared to the TV model, much better JS values are obtained by our model. Both examples demonstrate that TV_p regularization functions better than TV regularization for segmentation of image corrupted by intensity inhomogeneity.

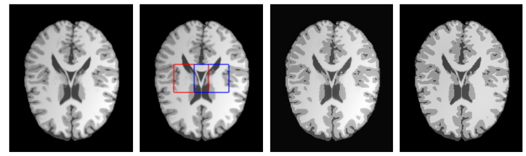

(a) Input (b) Initial (c) TVp g (d) TV g

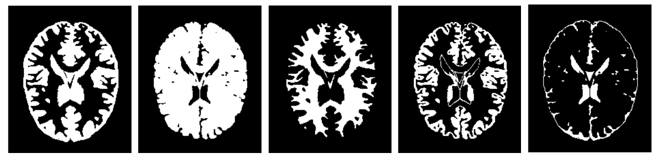

(e) TVp model

(f) TV model

Fig. 4. From left to right: u_1, u_2, WM, GM and CSF.

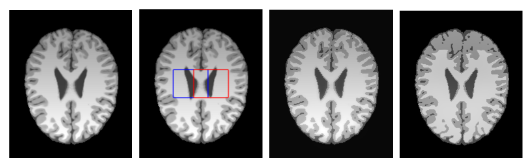

(a) Input (b) Initial (c) TVp g (d) TV g

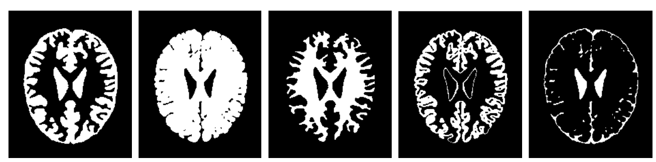

(e) TVp model

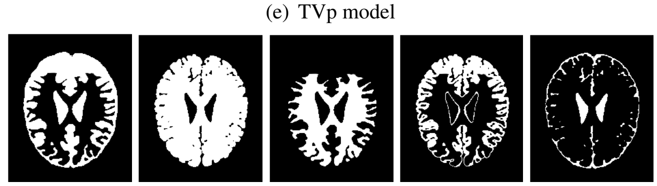

(f) TV model

Fig. 5. From left to right: u_1, u_2, WM, GM and CSF.

Table 2. JS of brain MR images.

Methods	Fig. 4			Fig. 5		
	WM	GM	CSF	WM	GM	CSF
TVp model	**97.40**	**91.92**	**92.61**	**96.38**	**89.58**	**89.12**
TV model	91.00	83.53	90.86	78.82	66.79	81.71

4. CONCLUSION

In this paper, we presented a novel piecewise smooth segmentation approach by modeling the true image as a sum of a piecewise constant function and a smooth function. The sparsity was enforced on both image gradient and data fidelity. An efficient minimization algorithm based on the ADMM strategy has been developed to solve the proposed model. Experiments have demonstrated its good performance.

5. REFERENCES

[1] David Mumford and Jayant Shah, "Optimal approximations by piecewise smooth functions and associated variational problems," *Communications on Pure and Applied Mathematics*, vol. 42, no. 5, pp. 577–685, 1989.

[2] Tony F Chan and Luminita A Vese, "Active contours without edges," *IEEE Transactions on Image Processing*, vol. 10, no. 2, pp. 266–277, 2001.

[3] Stanley Osher and James A Sethian, "Fronts propagating with curvature-dependent speed: algorithms based on hamilton-jacobi formulations," *Journal of Computational Physics*, vol. 79, no. 1, pp. 12–49, 1988.

[4] Luminita A Vese and Tony F Chan, "A multiphase level set framework for image segmentation using the mumford and shah model," *International Journal of Computer Vision*, vol. 50, no. 3, pp. 271–293, 2002.

[5] Johan Lie, Marius Lysaker, and Xue-Cheng Tai, "A variant of the level set method and applications to image segmentation," *Mathematics of Computation*, vol. 75, no. 255, pp. 1155–1174, 2006.

[6] Tony F. Chan and Mila Nikolova, "Algorithms for finding global minimizers of image segmentation and denoising models," *SIAM Journal on Applied Mathematics*, vol. 66, no. 5, pp. 1632–1648, 2006.

[7] Egil Bae, Jing Yuan, and Xue Cheng Tai, "Global minimization for continuous multiphase partitioning problems using a dual approach," *International Journal of Computer Vision*, vol. 92, no. 1, pp. 112–129, 2011.

[8] J Lellmann and C Schnörr, "Continuous multiclass labeling approaches and algorithms," *SIAM Journal on Imaging Sciences*, vol. 4, no. 4, pp. 1049–1096, 2011.

[9] Triet Le and Luminita Vese, "Additive and multiplicative piecewise-smooth segmentation models in a variational level set approach," *Contemporary Mathematics*, vol. 445, pp. 207–224, 2007.

[10] Miyoun Jung, "Piecewise-smooth image segmentation models with L1 data-fidelity terms," *Journal of Scientific Computing*, vol. 70, no. 3, pp. 1229–1261, 2017.

[11] William M Wells, W Eric L Grimson, Ron Kikinis, and Ferenc A Jolesz, "Adaptive segmentation of mri data," *IEEE Transactions on Medical Imaging*, vol. 15, no. 4, pp. 429–442, 1996.

[12] Chunming Li, Rui Huang, Zhaohua Ding, Chris Gatenby, Dimitris Metaxas, and John Gore, "A variational level set approach to segmentation and bias correction of images with intensity inhomogeneity," in *International Conference on Medical Image Computing and Computer-Assisted Intervention*. Springer, 2008, pp. 1083–1091.

[13] Alessandro Lanza, Serena Morigi, and Fiorella Sgallari, "Constrained TVp model for image restoration," *Journal of Scientific Computing*, vol. 68, no. 1, pp. 64–91, 2016.

[14] E. Y. Sidky, R Chartrand, J. M. Boone, and X. Pan, "Constrained TpV minimization for enhanced exploitation of gradient sparsity:application to CT image reconstruction," *IEEE Journal of Translational Engineering in Health & Medicine*, vol. 2, no. 6, pp. 1–18, 2014.